

# **Investigation of the co-crystallisation of N-heterocycles**

**By**

**Leigh-Anne Loots**

*Thesis presented in partial fulfilment of the requirements for the  
degree of Master of Science*



*Stellenbosch University*

Department of Chemistry and Polymer Science

Faculty of Science

Supervisor: Leonard J. Barbour

March 2009

**$\alpha$ -O3N3 (1:1)**

The ASU of  $\alpha$ -O3N3 (Figure 3.58) is comprised of one molecule each of resorcinol and pyrimidine in the triclinic space group  $P\bar{1}$ . The thermal ellipsoids shown in Figure 3.58 are not ideally shaped and this is possibly due to deterioration of the crystal during data collection. The two molecules are approximately co-planar with the hydroxyl groups of resorcinol positioned in the *syn-anti* conformation so as to form H-bonded chains,  $C_2^2(10)$ , with alternating pyrimidine molecules.

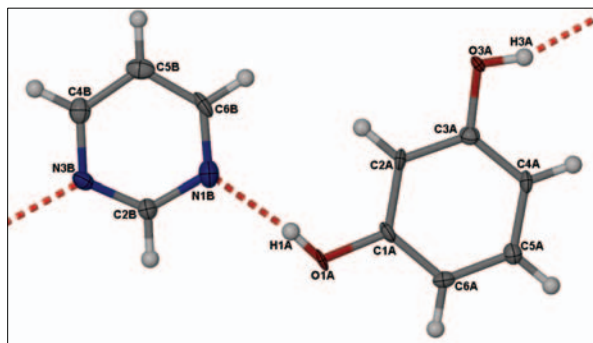


**Figure 3.58** Thermal ellipsoid plot of the ASU of  $\alpha$ -O3N3.

Adjacent chains are slightly staggered along [010], but form a 2-D layer with C–H $\cdots$ O (short tails in Figure 3.59) interactions between polymeric chains to form a 2-D layer. The 2-D layers simply stack on top of one another with offset  $\pi$ - $\pi$  interactions between resorcinol and pyrimidine in adjacent layers (shown as a green area on the diagonal (1.7 Å) in Figure 3.59).

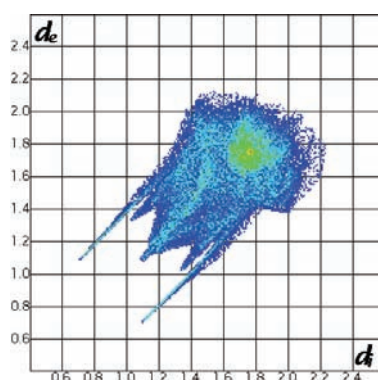


**Figure 3.59** Fingerprint plot of  $\alpha$ -O3N3.

Owing to the instability of  $\alpha$ -O3N3 at ambient temperatures it was not possible to perform PXRD analysis on the bulk material. SDG experiments were carried out in an attempt to reproduce the co-crystal. The results obtained are shown in Figure 3.60, demonstrating that the SDG pattern is somewhat comparable to the pattern simulated from the single-crystal data, but there are two additional peaks (at ca 8° 2 $\theta$  and 18° 2 $\theta$ ) in the experimental pattern, possibly from the start of conversion to the  $\beta$ -form.

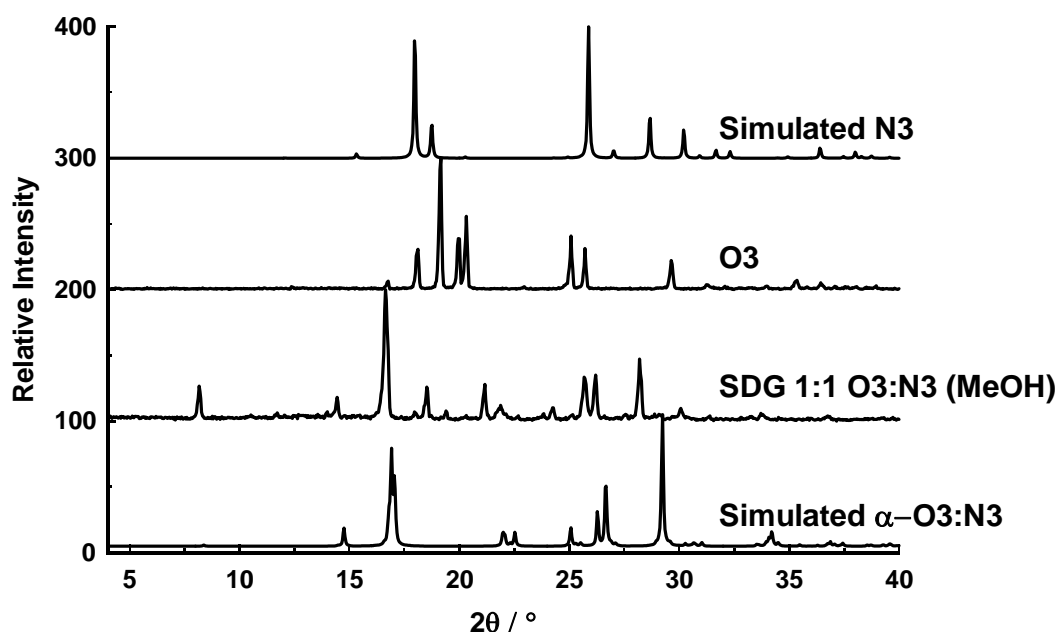


**Figure 3.60** PXRD analysis of a SDG experiment of O3N3 in a 1:1 ratio using methanol as solvent, compared to the simulated pattern of  $\alpha$ -O3N3 and the two patterns of the two starting materials.

### $\beta$ -O3N3 (2:1)

The ASU of  $\beta$ -O3N3 consists of two molecules of resorcinol and a single molecule of pyrimidine (Figure 3.61), in the monoclinic space group  $P2_1/c$ . Polymeric chains,  $C_2^2(10)$ , analogous to those in  $\alpha$ -O3N3, are formed by H-bonding of molecules A and C, making use of the  $O-H \cdots N_{\text{arom}}$  synthon.

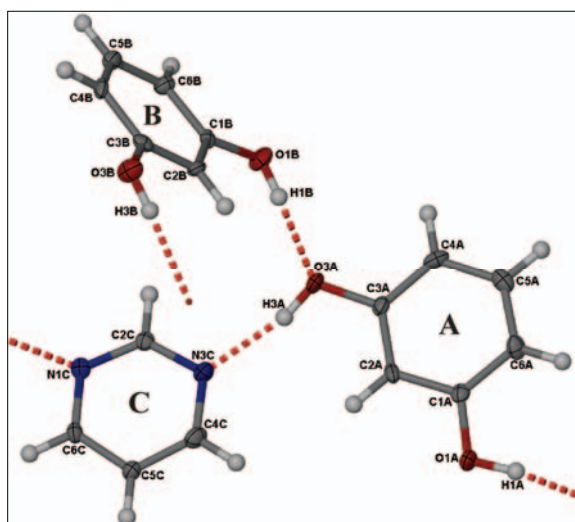


**Figure 3.61** Thermal ellipsoid plot of the ASU of  $\beta$ -O3N3 showing resorcinol in two (*syn-syn* and *syn-anti*) out of the three possible conformations.

The  $\beta$ -O3N3 structure has a more robust 3-D architecture than the  $\alpha$ -form, with a second, crystallographically independent resorcinol molecule maintaining the positions of two chains

running *anti*-parallel to each other. Molecule **B** adopts the *syn*-*syn* conformation and acts as a pincer, keeping the array relatively rigid (Figure 3.62). The chains, however, are not separated by the maximum distance possible for the pincer resorcinol. It is assumed that there is a compromise between the orientation of the pincer resorcinol and favourable  $\pi\cdots\pi$  interactions between adjacent chains. In order for there to be favourable  $\pi\cdots\pi$  interactions between molecules **A** and **C**, the resorcinol pincer is forced to twist in order to hydrogen bond to two nearby resorcinol molecules in the adjacent chains.

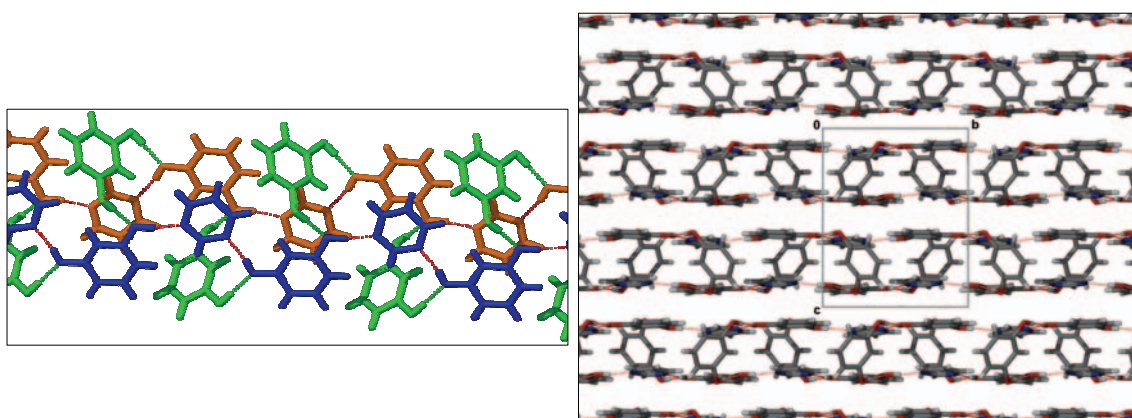


**Figure 3.62** The two *anti*-parallel chains (orange and blue represent separate chains) pinched by *cis*-oriented resorcinol molecules (green) are shown on the left. These double chains then pack along the *c* axis as shown on the right.

Two of the three possible conformations of resorcinol are observed in the  $\beta$ -O3N3 co-crystal. The *syn*-*anti* conformer (**A**) forms part of the polymeric chain similar to that in  $\alpha$ -O3N3, while the *syn*-*syn* conformer (**B**) is used to stabilise the structure by pinching two polymeric chains together in an *anti*-parallel manner. Therefore, **A** acts as both a hydrogen bond donor and acceptor molecule, while **B** donates only to molecule **A**. This is another example where a structure forms in a non-equimolar ratio, and an additional donor molecule is involved in hydrogen bonding with the dual donor-acceptor resorcinol molecule (**A**).

The fingerprint plot identifies three main interactions in the structure of  $\beta$ -O3N3 – the O-H $\cdots$ N hydrogen bonds (outer tails) that overlap with the C-H $\cdots$ O tails in Figure 3.63 and the  $\pi\cdots\pi$  interaction, illustrated by the green area on the diagonal at 1.8 Å.

A SDG experiment carried out using an equimolar ratio of the co-crystal components and a few drops of water yielded solid material with a

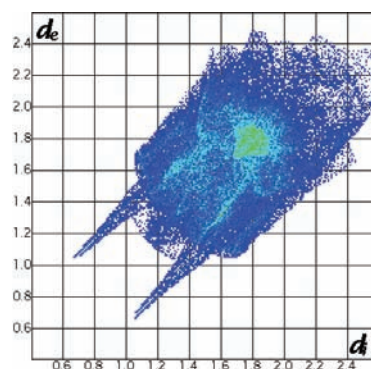


**Figure 3.53** Fingerprint plot of  $\beta$ -O3N3

diffractogram that is a close match to the pattern simulated from single-crystal data of  $\beta$ -O3N3 (Figure 3.64). DSC analysis (Figure 3.65) of this SDG product shows two thermal events that occur in succession. The first occurs at  $T_{\text{on}} = 48\text{ }^{\circ}\text{C}$  and the second begins directly after the first, at  $T_{\text{on}} = 55\text{ }^{\circ}\text{C}$ . Without further information, it is difficult to speculate the cause for the twinned peak, although it may be due to a rearrangement of the molecules in the crystal structure.

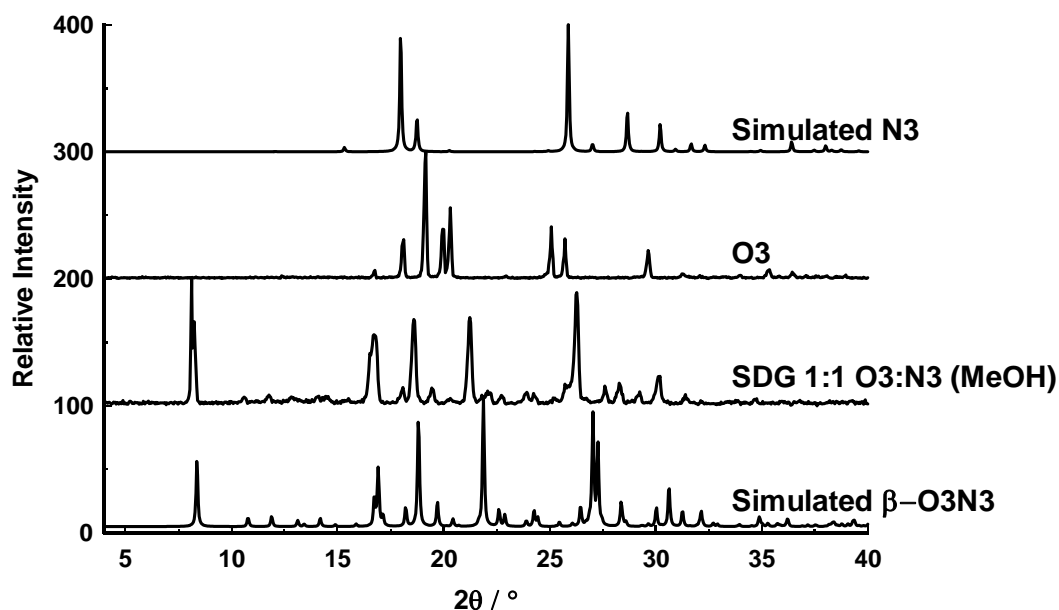


**Figure 3.64** The PXRD comparison of an equimolar SDG experiment, with  $\text{H}_2\text{O}$  as solvent, with the simulated  $\beta$ -O3N3 pattern and the two starting components.

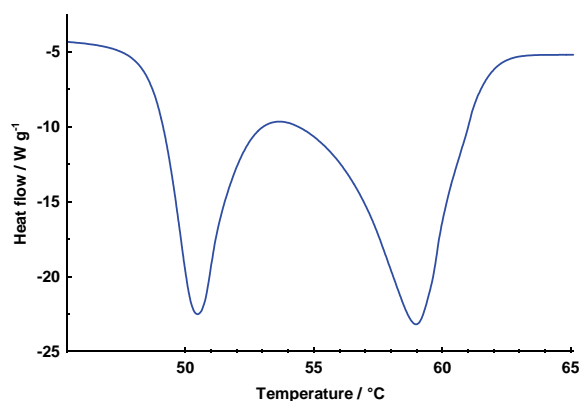
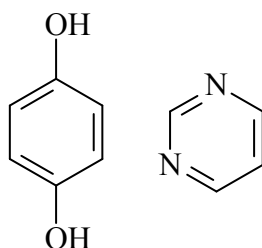


**Figure 3.65** DSC trace for 1:1 SDG of  $\beta$ -O3N3 with  $\text{H}_2\text{O}$  as solvent

## 3.2.6 O4N3 – Hydroquinone and pyrimidine (1:1 ratio)



Scheme 3.12 Co-crystal formers hydroquinone and pyrimidine

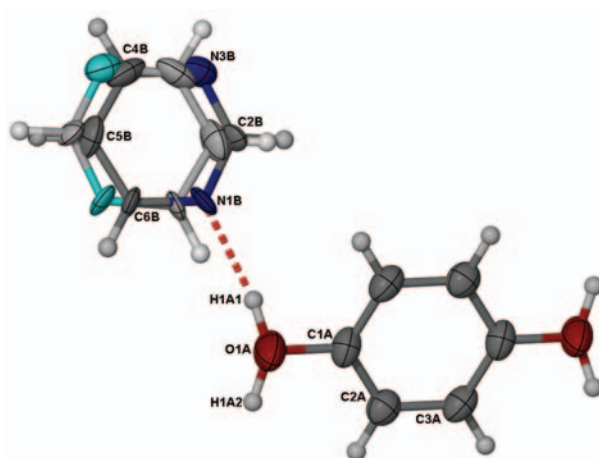


Figure 3.66 Thermal ellipsoid plot of modelled O4N3. Only the ASU is labelled.

The structure O3N3 presents an interesting example of disorder and leads to the question: what if X-ray crystallography is unable to distinguish between two possible H-bonding motifs? This particular structure exhibits disorder of the hydroxyl hydrogen atoms as well as the positions of the nitrogen atoms in the pyrimidine ring. Bond lengths and angles were used as a basis to model the structure to a good approximation of one that is plausible.

After routine structure solution and refinement a model consisting of half a molecule of hydroquinone situated on a position of  $\bar{1}$  site symmetry at  $\frac{1}{4}, \frac{1}{4}, 0$  and half a pyrimidine molecule situated on a diad at  $\frac{1}{2}, y, \frac{1}{4}$  was found in the ASU (Figure 3.66). Owing to symmetry-imposed disorder, the structure was modelled by duplicating the pyrimidine ring and fixing the bond distances of each ring using values obtained from a CSD analysis of the pyrimidine molecule. Each pyrimidine molecule is assigned 50% site occupancy. The hydroxyl hydrogen atoms of hydroquinone are disordered over two positions, and each was fixed at a standard bond distance (0.95 Å) and assigned a 50% site occupancy factor.

A detailed analysis of possible hydrogen bonding patterns that are consistent with the disordered model yields two distinct possibilities with practically identical packing

arrangements. Both possibilities involve assembly of the two molecular components into two dimensional layers that propagate parallel to (10-1). Within these layers, intermolecular interactions are dominated by O–H $\cdots$ N and C–H $\cdots$ O hydrogen bonds, but no interactions other than relatively weak dispersive forces appear to bind adjacent layers together. Therefore, most of the discussion that follows will be confined to the hydrogen-bonded interactions that occur within ordered domains of the two-dimensional layers.

We suggest that the observed disorder is static rather than dynamic, and that individual layers do not dictate the symmetry of the subsequent layers. Owing to weak interlayer interactions, the hydrogen-bonding pattern within one layer most likely does not influence that within an adjacent layer, and the disorder thus results from a statistical distribution of possibilities.

To determine a chemically feasible packing arrangement with relevant hydrogen bonding taken into consideration, we need to consider that the disordered crystallographic model

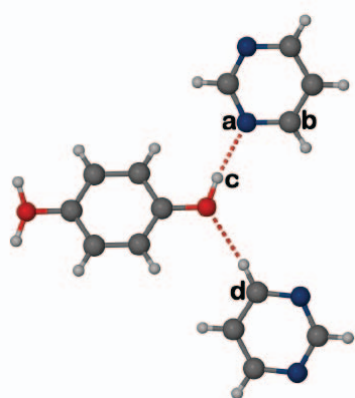


**Figure 3.67** Arbitrarily labelled atoms *a*, *b*, *c* and *d* of O4N3.

supports two possible positions for (i) the hydrogen atom of each hydroxyl group of each hydroquinone molecule, and (ii) each of the two nitrogen atoms in the pyrimidine heterocycle. It follows that, for hydrogen bonding to take place between these two molecules, the disordered atoms can only occupy one of the two possible positions at any point in time.

Considering the hydrogen atom of the hydroxyl group – if it is positioned in one direction (*c*, Figure 3.67), it follows that the pyrimidine must be positioned such that the nitrogen atom (*a*, Figure 3.67) may interact with the hydrogen bond donor forming an O–H $\cdots$ N hydrogen bond. This in turn necessarily controls the orientation of another nearby pyrimidine molecule such that a C–H $\cdots$ O (*d*, Figure 3.67) interaction is observed between the diazine and hydroquinone. This holds true for both hydroxyl groups. However, it must be considered that the hydroxyl hydrogen atoms of any given hydroquinone molecule may be positioned either *cis* or *trans* with respect to one another. Considering this, we are presented with two possible hydrogen-bonding patterns. If the *cis*-conformation (*a*, Figure 3.68 (left)) is assumed then it follows that the two pyrimidine molecules must both be oriented such that their nitrogen atoms face towards each other (*e*, Figure 3.68 (left)). Consequently the entire array will consist of identical hydrogen bonded rings (*acdb*),  $R_4^4(22)$ , in which the molecules are linked by relatively strong O–H $\cdots$ N hydrogen bonds. Weaker C–H $\cdots$ O

interactions are then responsible for retaining the rings in position within the 2-D layer. As a result of the ring arrangement, the orientations of pyrimidine molecules are alternated both vertically (blue band, Figure 3.68 (left)) and horizontally (red band, Figure 3.68 (left)).

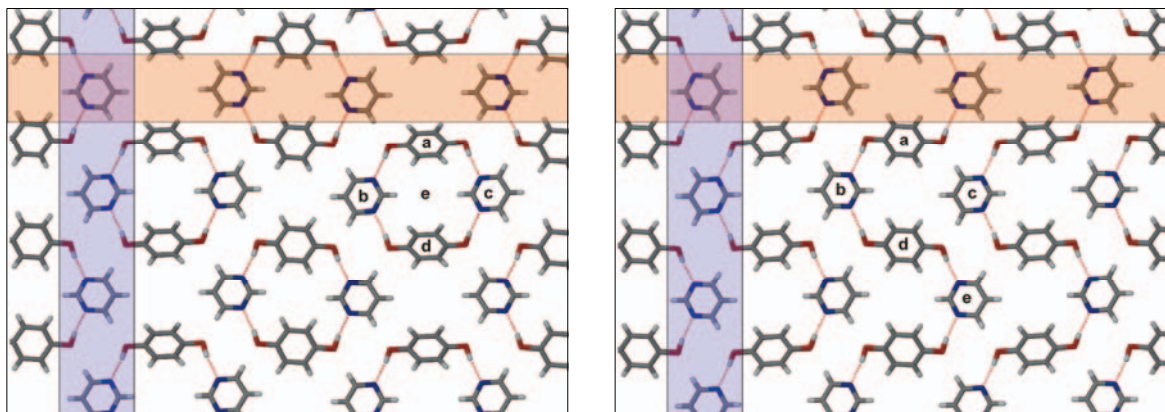


**Figure 3.68** *Cis*-conformation of hydroquinone with the resultant ring formation centred around *e* on the left. The *trans*-conformation and resulting hydrogen bonded chains are represented on the right. Both are viewed down [001]. Red bands show the differing alignments of pyrimidine within a row of the *cis* and *trans* representations. Blue bands show the similar alternation of pyrimidine along the vertical.

If we assume the *trans*-conformation for any given molecule of hydroquinone, there will be only a slight change in the localised hydrogen bonding pattern, the overall pattern within the 2-D layer, however, is quite different. We find that the hydrogen bonded pathway between *a*  $\cdots$  *b*  $\cdots$  *d* is maintained and then, owing to the *trans*-conformation of the second hydroxyl group, molecule *c* is no longer involved in the local hydrogen bonding pattern, but rather *d* bonds to *e*, thus forming a conceptually infinite chain,  $C_4^4(22)$ . In this array, the vertical arrangement of pyrimidine molecules is identical to that seen for the *cis*-conformation (Figure 3.68), while horizontally they have a polar arrangement within a row, and adjacent horizontal bands are oriented in an *anti*-parallel fashion. Because the structure is disordered it becomes difficult to identify any secondary interlayer interactions that may be of importance to the 3-D arrangement and it is thus assumed that these interactions are of little consequence to the overall packing of the molecules. From this point forward, the packing arrangement adopted for the *trans* conformation is referred to as Scenario 1, while the *cis* conformation is assigned Scenario 2.

Without other supporting analytical techniques to distinguish between the two different scenarios, a preferred model must be chosen that makes chemical sense. In an effort to discern which H-bonding pattern is prevalent in the lattice, samples were submitted for MAS-NMR analysis to determine a more accurate position of the hydroxyl hydrogen atom. Three samples with different hydroquinone conformations were analysed for comparative



purposes. The  $\alpha$ -O4N2 co-crystal was selected as a *trans*-conformer, a co-crystal (not presented here) in which hydroquinone exists as the *cis*-conformer and the sample of interest, O4N3, in which the conformation is ambiguous.  $^{13}\text{C}$  as well as  $^1\text{H}$  spectra were obtained on a 500 MHz instrument using a 6 mm probe spinning at 8 kHz. Due to the low resolution of the peaks in the  $^1\text{H}$  spectra, the results obtained did not facilitate differentiation between the two conformations. Samples have subsequently been sent to Prof. John Ripmeester at the Steacie Institute for Molecular Sciences (SIMS) in Canada for a more detailed analysis using 900 MHz MAS-NMR instrumentation. The results of these experiments are still pending.

Chemical modelling of both Scenarios were carried out by Dr Catharine Esterhuysen to determine whether one arrangement is energetically more favourable than the other. The two factors considered to play a role in stabilising the different packing modes are (1) the difference in the relative hydrogen atom orientations of the hydroxyl groups of hydroquinone (*cis* or *trans*) and (2) the differences between  $\text{O-H}\cdots\text{C}$  and  $\text{O-H}\cdots\text{N}$  hydrogen bond stabilisations for the two different orientations. Concerning (1) the energies of the two conformations are near equivalent with the *trans*-conformation being only  $0.5 \text{ kcal mol}^{-1}$  lower in energy than the *cis*-conformation. In the case of (2), the hydrogen bond strength of the  $\text{O-H}\cdots\text{N}$  is almost identical in all cases, approximately  $7.8 \text{ kcal mol}^{-1}$  each, with those found in Scenario 1 being slightly stronger ( $0.1 \text{ kcal mol}^{-1}$  lower in energy). The  $\text{O-H}\cdots\text{C}$  interactions are found to be slightly destabilising, being approximately  $0.1 \text{ kcal mol}^{-1}$  higher in energy in Scenario 1, thus negating the additional  $\text{O-H}\cdots\text{N}$  stabilisation and leading to the two different packing modes being practically identical in energy. A ratio of 62:38 of Scenario 1 to Scenario 2 is expected utilising the Boltzmann equation.

Powdered material of O3N3 is easily obtained by grinding the two components in the presence of a few drops of methanol and the PXRD pattern of the product is comparable to that simulated from the single-crystal data (Figure 3.69). A 1:2 SDG product appears to undergo incomplete conversion, resulting in a mixture of the two starting materials. The melting point of the product can be established by DSC analysis, corresponding to the single thermal event  $T_{\text{on}} = 89 \text{ }^\circ\text{C}$  (Figure 3.70).

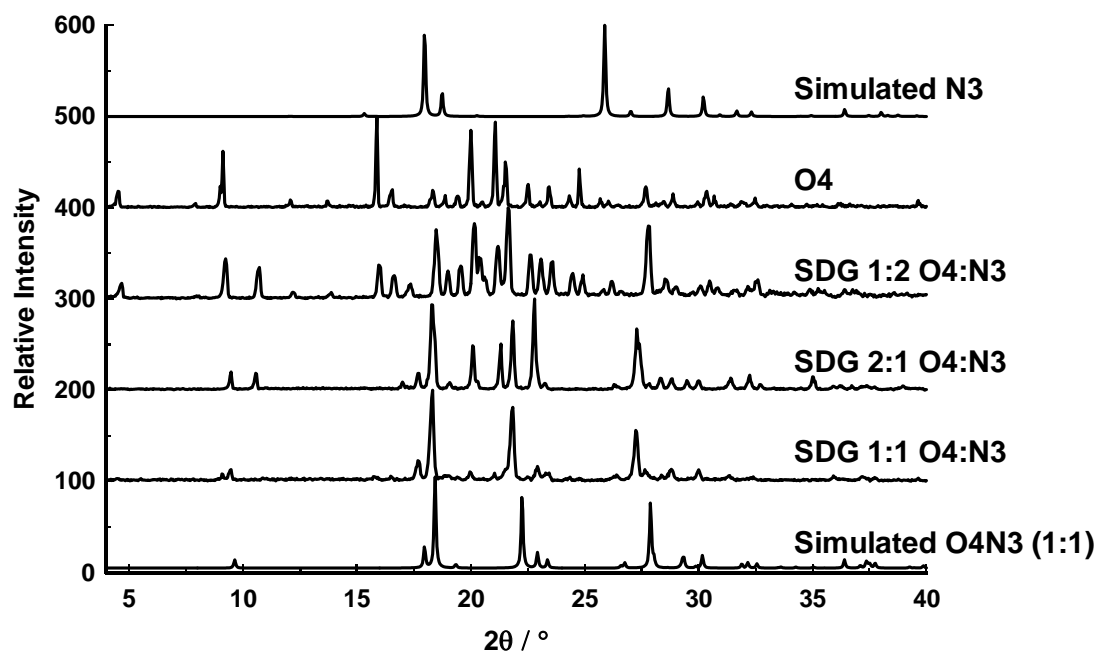


**Figure 3.69** A comparison of the simulated PXRD pattern of O4N3 with the SDG experimental patterns and the two starting materials.

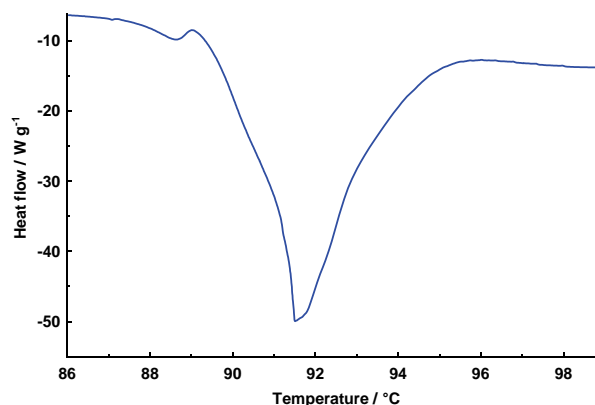
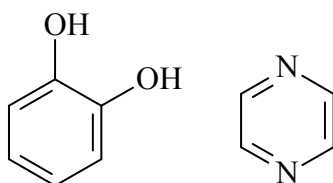


**Figure 3.70** DSC trace of co-crystal O4N3

### 3.2.7 O2N4 – Catechol pyrazine (2:1 ratio)



**Scheme 3.13** Co-crystal formers catechol and pyrazine

The ASU of O2N4 (Figure 3.71) consists of two catechol molecules and a single molecule of pyrazine, crystallising in the orthorhombic space group *Pbca*. The existence of slightly different dihedral angles between the pyrazine and catechol molecules accounts for the large ASU and the structure was checked for missing symmetry to confirm the correct space group

assignment. Two different hydrogen-bonding motifs are utilized to form chains that propagate along the  $a$  axis. A hydrogen bonded ring,  $R_2^2(10)$ , is formed *via* O–H $\cdots$ O interactions between two symmetry-independent catechol molecules. Pyrazine connects the symmetry-independent catechol molecules using the heterosynthon OH $\cdots$ N<sub>arom</sub> to form H-bonded chains,  $C_4^4(12)$ , as shown in Figure 3.74 (top).

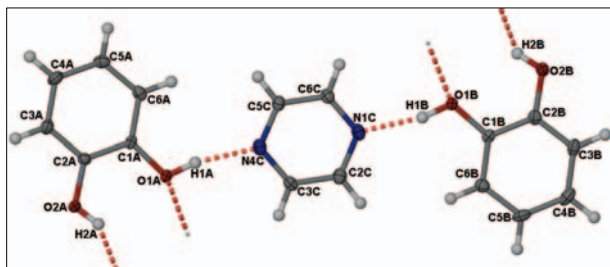


**Figure 3.71** Thermal ellipsoid plot of the ASU of O2N4

The packing arrangement involves chains propagated along [100] that interact with adjacent chains *via* C–H $\cdots$  $\pi$  interactions (wings in Figure 3.72). These C–H $\cdots$  $\pi$  interactions facilitate packing of the chains in a herringbone motif (Figure 3.73).

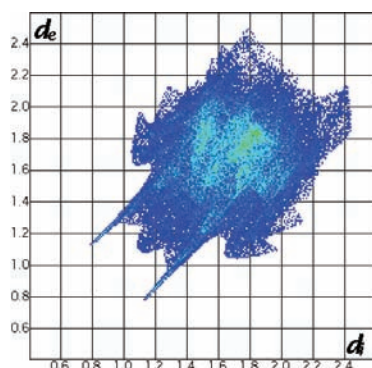


**Figure 3.72** Fingerprint plot of O2N4

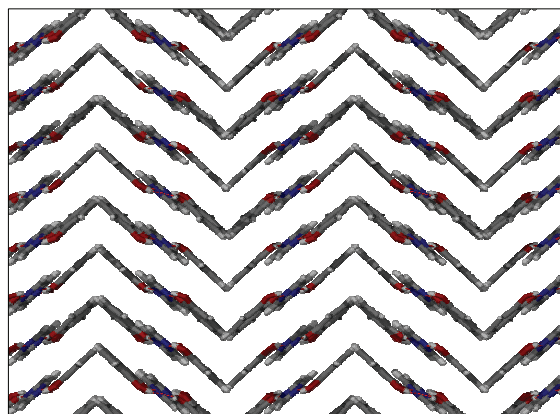


**Figure 3.73** Herringbone motif adopted by O2N4 owing to C–H $\cdots$  $\pi$  interactions, viewed along [100]

The 1-D chains resemble those formed in the structure of pure catechol (O2) in section 3.1.1. However, in the O2 structure chains are more branched owing to the dual donor-acceptor capabilities of catechol. This similarity suggests that the pyrazine molecules simply replace some of the catechol molecules already present in order to insert themselves into the array.

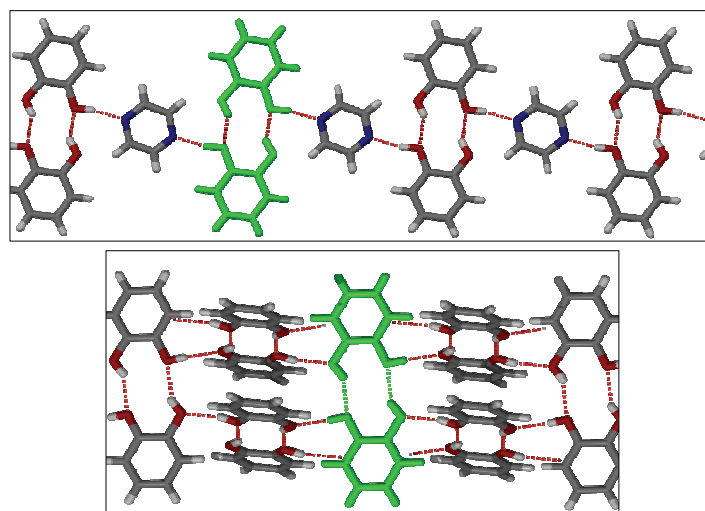


**Figure 3.74** Hydrogen bonded chain showing the ring formation between catechol molecules in O2N4 (top) and the analogous ring formation in catechol (O2).

A 1:1 SDG experiment yields a PXRD pattern comparable to the simulated pattern obtained from O2N4 single-crystal data (Figure 3.75). A different pattern was obtained when SDG experiments were carried out using an excess of either of the two starting materials. Single-crystal data for this compound have not yet been obtained. The DSC trace (Figure 3.76) of the 1:1 SDG product reveals a thermal event in the range 69-76 °C. A single thermal event is observed during the first cycle of the procedure, while the second cycle produces a split peak, possibly due to a phase transformation to a more thermally stable product. This product may or may not correspond to the unknown powder product, but a variable temperature PXRD is required for confirmation.

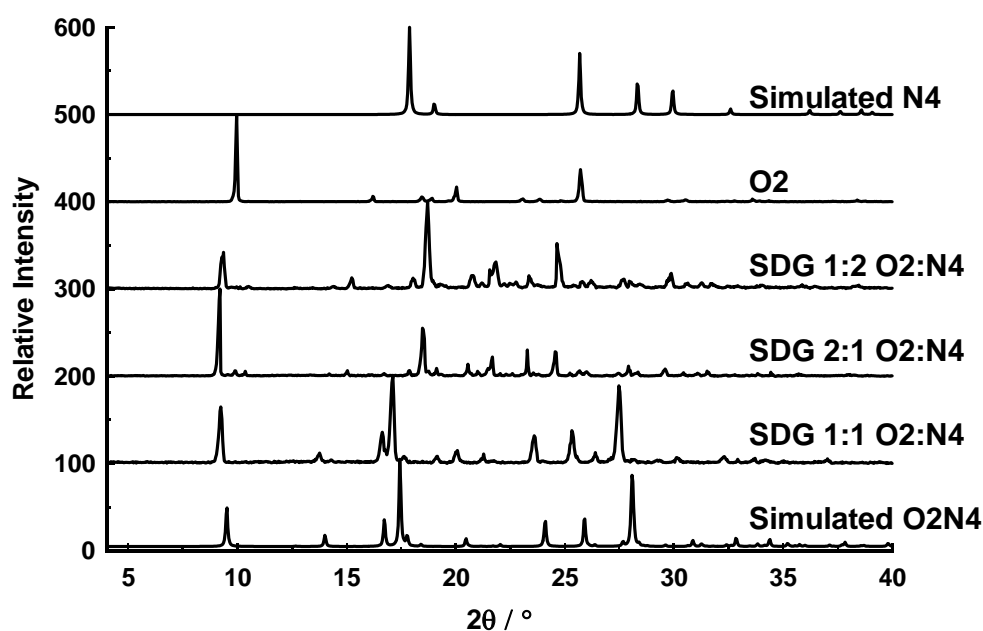


**Figure 3.75** Comparison of the simulated diffractogram of O2N4 with the equimolar SDG product. A second distinctive product is obtained in the SDG experiments using either a 1:2 or 2:1 molar ratio. These two patterns appear to be distinct from the two starting materials.

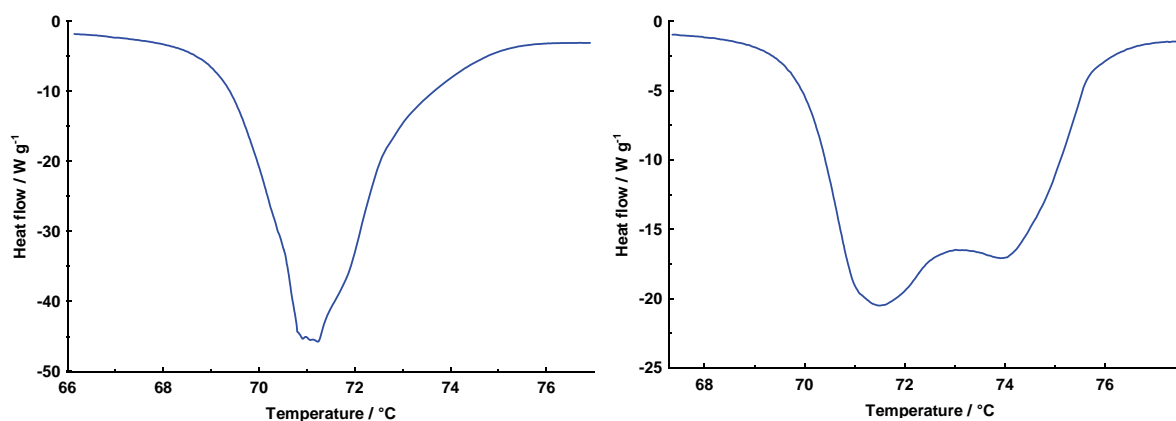
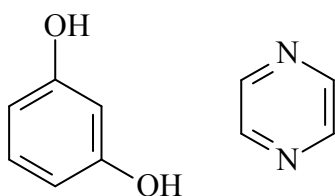


**Figure 3.76** DSC trace of O2N4. The first cycle (left) shows a single thermal event ( $T_{\text{on}} = 68\text{ }^{\circ}\text{C}$ ), while the second shows two consecutive thermal events ( $T_{\text{on}} = 70\text{ }^{\circ}\text{C}$  and  $73\text{ }^{\circ}\text{C}$ ).

### 3.2.8 O3N4 – Resorcinol pyrazine (1:1 and 3:1 ratios)



**Scheme 3.14** Co-crystal formers resorcinol and pyrazine

#### $\alpha$ -O3N4 (1:1)

One molecule each of resorcinol and pyrazine make up the ASU of  $\alpha$ -O3N4 in the monoclinic space group  $P2_1/n$ , (Figure 3.77). The *syn-syn* conformation is adopted by the resorcinol molecules in order to hydrogen bond with pyrazine in a 1:1 ratio to form a discrete quaternary adduct. This type of adduct is similar to those prepared for photodimerisation reactions as carried out in the MacGillivray<sup>6,17</sup> group. The pyrazine molecules in this instance are separated by  $3.9\text{ \AA}$ , just within the  $4.2\text{ \AA}$  limit for photo-induced reactions. However, the pyrazine heterocycles are not suitable for this type of reaction, since they are stable as aromatic molecules. The fingerprint plot (Figure 3.78) obtained indicates the presence of edge-to-face  $\pi$ -interactions as well as C–H $\cdots$ O interactions that organise adducts in 3-D. The edge-to-face interactions bring about a tight herringbone motif (Figure 3.79).

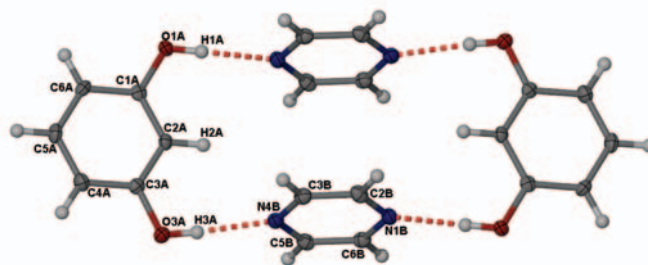


**Figure 3.77** Thermal ellipsoid plot of the quaternary adduct of  $\alpha$ -O3N4. Atoms of the ASU are labelled.

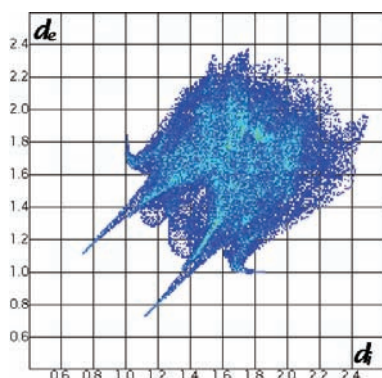


Figure 3.78 Fingerprint plot of  $\alpha$ -O3N4

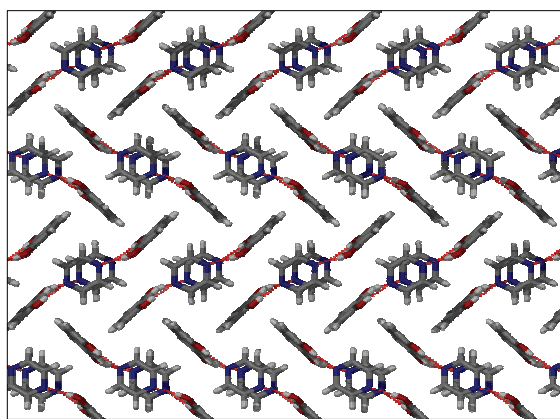


Figure 3.79 Packing diagram of  $\alpha$ -O3N4 showing a contracted herringbone motif (viewed along [100]).

The simulated PXRD of  $\alpha$ -O3N4 is in good agreement with the experimental SDG patterns (Figure 3.80) obtained for both 1:1 and 1:2 molar ratios. In this instance, an excess of pyrazine has no effect on the product formed. The DSC trace (Figure 3.81) shows two thermal events during the first cycle of the procedure, with only one event during the second cycle.

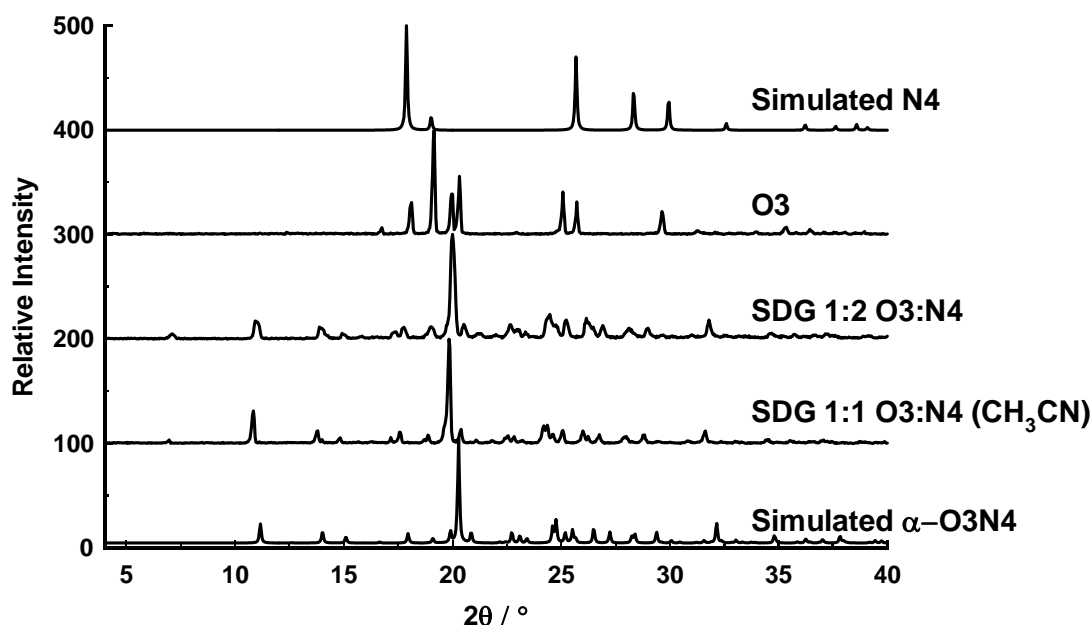
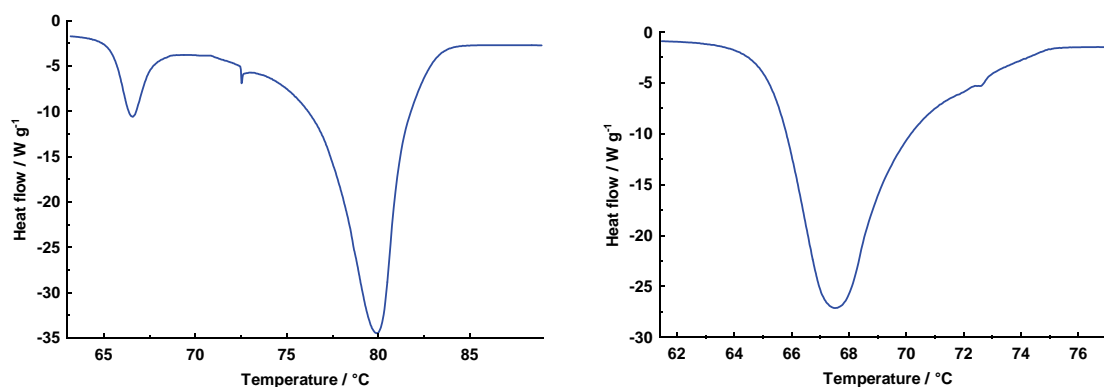


Figure 3.80 Simulated PXRD pattern of  $\alpha$ -O3N4 compared to the experimental patterns of 1:1 and 1:2 SDG products and the two starting materials pyrazine and resorcinol.



**Figure 3.81** DSC trace of  $\alpha$ -O3N4. Cycle 1 (left) shows two thermal events  $T_{\text{on}} = 65\text{ }^{\circ}\text{C}$  and  $76\text{ }^{\circ}\text{C}$ . Cycle 2 (right) exhibits a single thermal event  $T_{\text{on}} = 65\text{ }^{\circ}\text{C}$ .

### $\beta$ -O3N4 (3:1)

The  $\beta$ -form of O3N4 crystallises in the monoclinic space group  $P2_1/n$  with three symmetry-independent resorcinol molecules and a single pyrazine molecule in the ASU (Figure 3.82). All three resorcinol molecules adopt the *anti-anti* conformation. The *anti-anti* conformation is most like that of pure resorcinol and appears to create a more open framework. This is exemplified here by the 3-D arrangement composed of three interdigitated 3-D ladders. Interdigitation of the

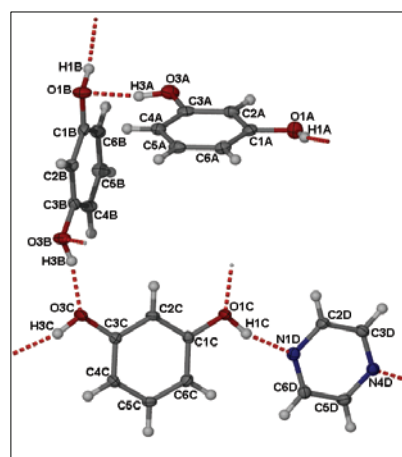


**Figure 3.82** Thermal ellipsoid plot of the ASU of  $\beta$ -O3N3 showing three resorcinol molecules, all in the *anti-anti* conformation.

ladders creates a more dense ( $1.357\text{ g cm}^{-3}$ ) structure than the  $\alpha$ -resorcinol ( $1.311\text{ g cm}^{-3}$ ). The insertion of pyrazine seems to impose a more ordered arrangement compared to that of  $\alpha$ -resorcinol, while at the same time preventing close packing. To interpret the structure, it is deconstructed into simpler hydrogen bonding motifs. The easiest portion to distinguish is the 1-D polymeric chain,  $C_2^2(11)$ , that utilises the  $\text{OH}\cdots\text{N}_{\text{arom}}$  synthon between resorcinol and pyrazine. These chains run parallel to the  $bc$  plane and are linked *via* hydrogen bonded rings,  $R_4^4(24)$ , along the  $ab$  plane. This linkage forms 2-D ladders across the  $ab$  plane. A 3-D network is then established by another hydrogen bonded ring,  $R_4^4(24)$ , joining neighbouring 2-D ladders across the  $ac$  plane (Figure 3.83). Hydrogen bonded rings in both cases are comprised exclusively of resorcinol molecules. The linker across the  $ab$  plane acts as both donor and acceptor, while the 3-D linkages consist only of donor molecules. Three distinct 3-D ladders are formed in this manner and they interpenetrate (Figure 3.84) to make up the complete structure.

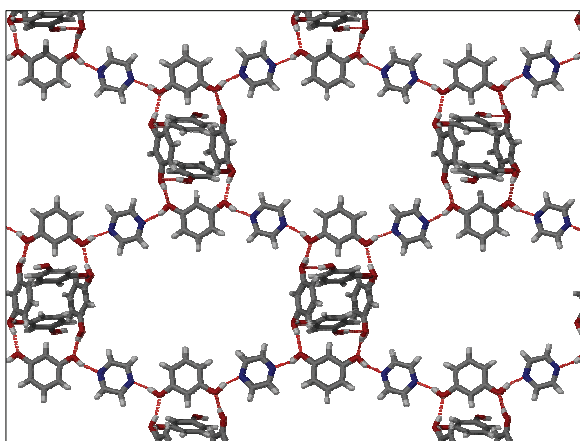


**Figure 3.83** A single 2-D ladder of O3N4

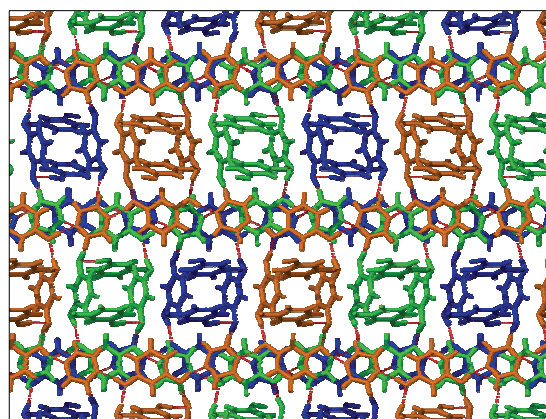


**Figure 3.84** Three interpenetrated 3-D ladders, depicted in orange, blue or green.

The fingerprint plot (Figure 3.85) illustrates the presence of the O–H $\cdots$ N and O–H $\cdots$ O interactions (overlapping tails) as well as  $\pi\cdots\pi$  interactions (light blue area along the diagonal at 1.8 Å) that play a lesser role in the packing arrangement. These  $\pi\cdots\pi$  interactions exist between neighbouring chain pyrazine and resorcinol molecules of interpenetrating structures.

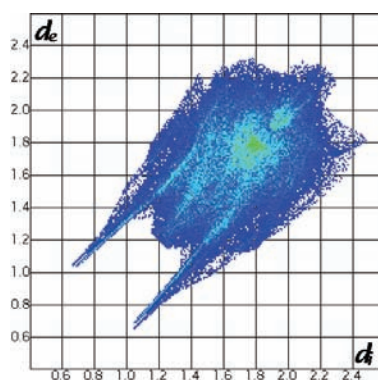


**Figure 3.85** Fingerprint plot of  $\beta$ -O3N4

The simulated PXRD pattern of  $\beta$ -O3N4 correlates well with that obtained from the analysis of a SDG experiment using a 2:1 molar ratio (Figure 3.86). Pyrazine was found to be relatively volatile during these experiments and this property provides an explanation for the difference in molar ratios of the starting and product materials. A single thermal event ( $T_{\text{on}} = 72\text{ }^{\circ}\text{C}$ ) is observed in the DSC trace (Figure 3.87) of  $\beta$ -O3N4.